Correlation between Double and Nonresonant Single Ionization

R. Wiehle and B. Witzel*

Department of Molecular and Optical Physics, Albert-Ludwigs-Universität Freiburg, Hermann-Herder-Strasse 3, 79104 Freiburg, Germany

(Received 10 May 2002; published 12 November 2002)

We performed simultaneous measurements of electrons and ions produced in Xe photoionization driven by an 800-nm, 100-fs laser pulse. The obtained energy and angular resolved electron spectra allow the identification of the electronic states populated during the ionization. Xe^{2+} ions appear at the same laser intensity as electrons emerging from a nonresonant 9-photon ionization process of Xe. Similar to optical tunneling ionization, the nonresonant ionization delivers low-energy electrons needed for the formation of Xe^{2+} by a backscattering process.

DOI: 10.1103/PhysRevLett.89.223002 PACS numbers: 32.80.Gc, 32.80.Rm, 39.30.+w

Since early experimental advances in laser-driven strong field double ionization of noble gases, a variety of theoretical approaches have been developed and new types of experiments have been performed to explore the details of such ionization processes [1–8]. In multiphoton double ionization the question arises whether the two electrons are ejected one after the other (sequentially), producing first a singly charged ion which is subsequently ionized, or simultaneously (nonsequentially). This topic has been discussed controversially since the 1970s. A characteristic feature of a nonsequential (NS) ionization process might be a knee structure in the curve describing the laser intensity dependence of the doubly charged ion yield. For the first time such a knee was found in the case of xenon [1] interacting with a 0.53-μm, 50-ps laser pulse. The knee was later ascribed to the occurrence of a resonance in the ionization scheme, because this feature is absent at 248-nm wavelength [9]. Multiphoton NS double ionization again received enhanced attention after it was observed in helium [2]. A high precision ion yield measurement, performed with a short pulse 800-nm Ti:sapphire laser, showed unexpectedly large amounts of doubly charged helium ions at low laser intensities. This observation cannot be explained by the Ammosow-Delone-Krainov theory [10] nor by a stepwise photoionization process.

The most likely scenario for NS double ionization in the near infrared regime is given by the rescattering model [11–13]. At first, an electron is set free by a laser-driven ionization process, after which it is accelerated and driven back by the laser field to its parent ion. The recollision with the electron causes an excitation or ionization of the ion. First indications of this process have been found by differential measurements of the doubly charged ion momentum and by coincidence measurements [14–16] of electrons originating from the double ionization process. The COLTRIMS method [17] allows the observation of a collective emission of both electrons to the same half sphere which supports the rescattering model. Rescattering with maximal impact energy can take place only if sufficiently slow electrons are created in the first ionization step. A typical process is a laser induced tunneling process known as optical field ionization (OFI). The energy of the backscattered electron gained from the laser field is a function of the laser intensity and strongly depends on the phase of the radiation field at the moment the electron was freed. Classical calculation shows that this mechanism allows the creation of electrons with energies up to $3.17U_p$ (U_p is the quiver energy of a free electron in the electric field of a laser focus). This value defines the minimum laser intensity for impact ionization of an ion A^+ in the ground state by a backscattered electron:

$$I_{\min}[\mathrm{W/cm^2}] = 3.4 \times 10^{12}\mathrm{IP}(\mathrm{A}^+)[\mathrm{eV}]/\lambda^2[\mu\mathrm{m}]$$

(with λ the wavelength of the laser, IP the ionization potential of the ion, and $I_{\min}$ the minimum laser intensity). Excitation of the ion by a multiple rescattered electron would reduce this threshold and allow the appearance of doubly charged ions at lower intensities. In addition, quantum-mechanically based calculations [18] demonstrate an enhancement of the nonsequential ionization process by tunneling of the second electron assisted by the return of the first one.

To date no experiments exist on the laser intensity dependence of a doubly charged ion yield in combination with signatures in the electron spectrum. It is the purpose of this Letter to demonstrate that combined electron ion spectroscopy (CEIS) provides a deeper understanding of laser-driven ionization. It emphasizes correlations between prominent features in photoelectron imaging spectra and the ion yield curves. Even in intensity regimes where the singly charged ion yield is dominated by the volume expansion, the CEIS technique allows the identification of new channels playing a role in the ionization dynamics. With this new experimental approach we examine the ionization of xenon with 800-nm radiation and demonstrate that nonresonant (NR) ionization of xenon plays a role in the formation of the doubly charged xenon

ion. Depending on the intensity of the laser, excited states are tuned into resonance with the 8-, 9-, or 10-photon dressed ground states. From these excited states the continuum can be reached with one photon. For increasing intensities, opening or closing of ionization channels will first occur at the focus, where volume effects can be neglected and hence the order of the ionization process can be determined. Our basic goal is to identify the electrons associated with the formation of doubly charged xenon ions. With the CEIS technique we are able to demonstrate that the 9-photon NR ionization process of xenon plays an important role in the formation of doubly charged xenon ions.

A Ti:sapphire laser system is used, delivering 100-fs, 800-nm pulses at a repetition rate of 1 kHz with a maximum energy of 1 mJ/pulse (shot-to-shot stability of 4%). The linearly polarized beam is focused into a spectrometer, consisting of a photoelectron imaging device to monitor the angular and energy distribution [19] and a time-of-flight spectrometer to measure the charge to mass ratio of the ion yield (resolution $m/\Delta m = 56$). Because of the high order processes studied here, the focal region can be considered to be a point source of electrons and ions. While the electrons expand from the interaction region, a dc electric field of 80 V/cm projects them onto a 50-mm diam chevron-type set of MCP's (multichannel plates) with a phosphor screen attached. A computer based video camera records the impact positions of the photoelectrons. A typical electron image accumulates the signal of 10^5–10^7 electrons. The images are deconvoluted in an Abelian transformation to yield angle-resolved velocity distributions of the photoelectrons [20]. The ions are accelerated in the opposite direction, detected with a MCP and recorded with a multistop card (time resolution = 0.5 ns). A calibration measurement was used to correct the different detection efficiencies for Xe^+ and Xe^{2+} ions at low impact energies. The partial xenon gas pressure was regulated with a variable leak in order to ensure a linear response for the Xe^+ and Xe^{2+} ions of the digital detection system ($\leq 10^{-2}$ events per laser shot and stop channel).

In order to study the dynamics of the ionization process we recorded CEIS measurements at different laser intensities. The right panel of Fig. 1 shows the intensity dependence of the Xe^+ and Xe^{2+} ion yields. The results obtained are in good agreement with measurements of Talebpour *et al.* [21]. Without adjustment of the intensity axis of our Xe^+ curve, we find a good overlap with their data. The solid line represents the result of an *S*-matrix calculation [22,23] and fits well with our result. The dashed line represents the Xe^{2+} yield according to the same calculation, not taking into account the NS contribution. In the left part of Fig. 1, the time-of-flight traces are shown for three different intensities together with the

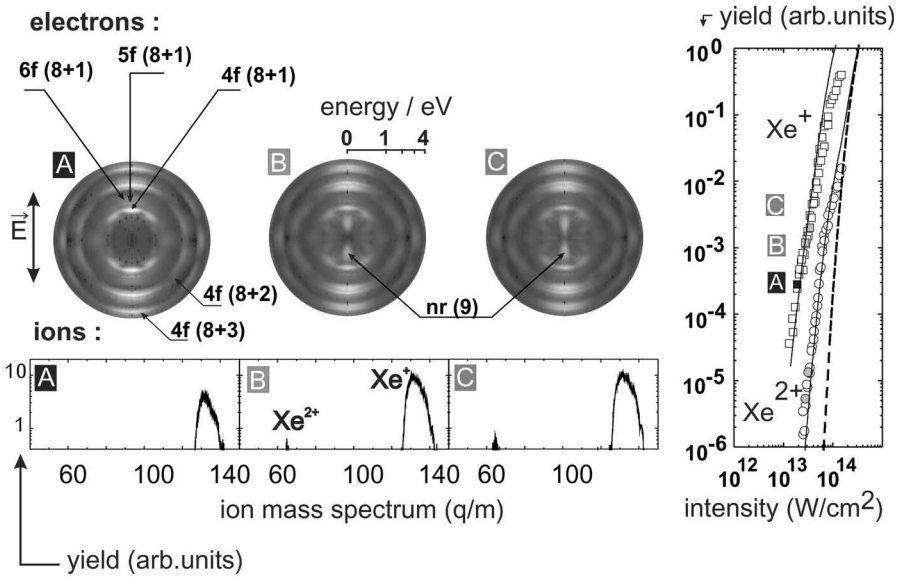

FIG. 1. CEIS spectra from xenon. Left part: momentum electron spectrum is shown together with the ion trace recorded by a time-of-flight mass spectrometer (laser: 800 nm, 100 fs). Intensities: (a) 2.2×10^{13} W/cm^2; (b) 3×10^{13} W/cm^2; (c) 3.3×10^{13} W/cm^2. The electron spectrum at (a) is mainly influenced by a 8 + 1 REMPI process via the $4f$, $5f$, and $6f$ states. Doubly charged xenon can be found at laser intensities higher than 3×10^{13} W/cm^2, where the electron spectrum is influenced by the 9-photon NR ionization process. Right part: dependency of the ionic yield as a function of the laser intensity. For comparison the result of the *S*-matrix theory for Xe^+ and Xe^{2+} is shown (solid line). The dashed line represents the calculation without the nonsequential part of the ionization.

momentum distribution of electrons in an energy range from 0 to 4 eV. Up to intensities of 2×10^{13} W/cm^2, excited states tune into resonance with an 8-photon dressed ground state, and excitation occurs to states from which the continuum can be reached with one photon. The energy signature of these photoelectrons is closely approximated by a picture that assumes ponderomotive shifting of the excited state $V_{Xe^*}[I]$ (I, laser intensity), as well as the ionization threshold IP. We expect a sharply peaked electron energy distribution with a maximum at $E = V_{Xe^*} - \mathrm{IP} + \hbar\omega$, because the difference $V_{Xe^*} - \mathrm{IP}$ does not depend on the laser intensity for high-lying Rydberg states. The high laser intensity allows the absorption of k additional photons in the last steps of the ionization process. The possible energies of the electron can be found at $E = V_{Xe^*} - \mathrm{IP} + k\hbar\omega$. The angular distribution of these electrons depends on the angular momentum of the resonant atomic state and on the number k of photons absorbed. The upper part of Fig. 1(a) is an example of an electron distribution strongly influenced by 8 + 1 REMPI (resonance enhanced multiphoton ionization) processes. The observed structures can be explained with populations of the $4f$, $5f$, and $6f$ Rydberg states during the laser interaction. All processes up to this laser intensity can be identified as MPI processes. Note that no low kinetic energy electrons are present at this intensity [Fig. 1(a) upper part]. At an intensity of 3.0×10^{13} W/cm^2 Xe^{2+} ions appear in the time-of-flight spectrum. The simultaneously recorded electron spectrum is shown in the upper part of Fig. 1(b). It contains new multilobed structures of low-energy electrons. The dominant lobes are pointing along the laser polarization. The simultaneous appearance of the doubly charged ions and the slow electron lobes strongly hints at an important role of such slow electrons in nonsequential double ionization.

Figure 2 (right part) shows in greater detail how the low kinetic energy part of the electron spectrum evolves for intensities increasing from 2×10^{13} W/cm^2 to 3.3×10^{13} W/cm^2. Below 2×10^{13} W/cm^2 no signal from low-energy electrons is found (center of the electron distribution). With increasing laser intensity, the minimum kinetic energy of the electrons decreases. This behavior can be understood by assuming a NR multiphoton ionization process, in which the decreasing electron energy results from an increased spacing between the ground state and the ionization threshold for increasing laser intensity [24,25]. The kinetic energy is then given by $E = n\hbar\omega - \mathrm{IP}[I]$, where n is the number of photons involved. The ponderomotively shifted IP at laser intensities between 2.3×10^{13} W/cm^2 and 3.2×10^{13} W/cm^2 ranges from 13.5 to 14.0 eV. The measured electron energies from 465 to 0 meV allow the identification of a 9-photon ionization. OFI can be excluded because the adiabatic parameter is about 2. At 3.8×10^{13} W/cm^2 we detect electrons resulting from a 9 + 1 REMPI

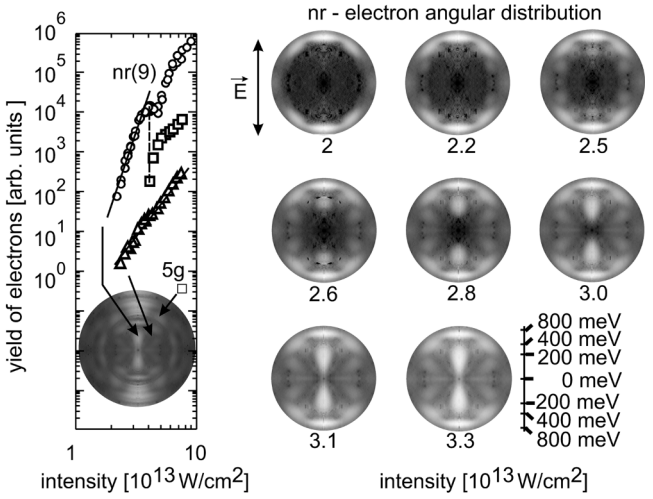

FIG. 2. Left: The electron yields as a function of the laser intensity from selected areas. These areas are shown in an electron image recorded at 3.8×10^{13} W/cm^2 (upper part). Rectangle: e^- yields from the 9 + 1 REMPI ($5g$) process. (For easier viewing, these data are moved down about 1.5 decades.) Circles: e^- yields from the nonresonant ionization. Triangles: yields of e^- emitted at an angle of 64° according to the polarization axes of the laser. The nonresonant process can be fitted with a line of a slope of about 9 and a straight line fitting the triangle has a slope of 4. Right: electron spectra as a function of the laser intensity.

process via the $5g$ state as an additional ring structure in the photoelectron imaging spectra (Fig. 2, left part) [26]. We integrated over the corresponding areas (NR and resonant) of the photoelectron spectra. For the NR process we count all electrons having kinetic energies below 465 meV and that are detected within ±10° from the direction of the laser polarization (open circles in Fig. 2, left part). For the resonant process ($5g$ state) the signal is integrated over a ring region, defined by $1.07eV \leq E_{\mathrm{kin}} \leq 1.31eV$ (open squares in the same figure). The NR process starts off with a slope of about 9 on the double logarithmic scale, which is compatible with a 9-photon ionization process. At low laser intensities the slope of about 9 can be found for the doubly charged xenon ions as well. At an intensity of 3.8×10^{13} W/cm^2 the electron yield of the NR process stabilizes. This is due to the opening of the 9 + 1 REMPI processes at this intensity [26].

Less prominent structures in Fig. 2, right part, are found to have different intensity dependencies. The kinetic energy of electrons ejected at an angle of 64° ± 10° with respect to the laser's polarization axis also decreases for increasing laser intensity, which is indicative of a NR process, but their yield curves have a slope of only 4 (Fig. 2, left part). Obviously more than one process contributes to the low kinetic energy part of the electron spectrum and causes this type of side lobe electrons. These results can be understood by referring to the

rescattering model, where low-energy electrons are needed for the excitation and ionization of the remaining singly charged ion. The low-energy electrons are a result of a NR 9-photon ionization and do not originate from an OFI process. The total process can be understood as a stepwise excitation of the xenon ion, due to multiple electron recollisions with Xe^+ and a final NR ionization process, schematically:

$$\begin{aligned} Xe &\rightarrow (Xe^+, e^-) \rightarrow (Xe^{*+}, e^-) \rightarrow \ldots \\ &\rightarrow (Xe^{*_n+}, e^-) \rightarrow Xe^{2+} + 2e^-. \end{aligned}$$

The first step is the ionization of xenon and the ejection of one electron. This electron is backscattered and excites the ionic core (Xe^{*+}). This process can be repeated several (n) times until the last step brings xenon into the doubly charged ionic continuum. The formation of Xe^{2+} has to occur via a stepwise excitation of Xe^+ by a multiscattered electron, because the ionization potential of Xe^+ (IP = 21.21 eV) is higher than the available impact energy (≤ 5.7 eV at 3×10^{13} W/cm^2). The first excited state of singly charged xenon $5p^5\,^2P_{1/2}$ is 1.3 eV above the ionization level of neutral xenon. The next higher-lying $5s^1\,5p^6$ state can be excited from the first excited state of the ion only with electrons having an impact energy of more than 9.96 eV. Such a high rescattering energy is not available at the intensity where we observe Xe^{2+}. Because the uncertainty of the laser intensity is less than 15%, we conclude that the observed ionization process cannot be understood by a simple excitation of the ion with a rescattered electron.

A different scenario ís the formation of doubly excited neutral xenon [27]. This can be achieved by recapturing of the ejected electron. Dielectronic recombination is enhanced in the presence of an electric field [28]:

$$Xe \rightarrow (Xe^+, e^-) \rightarrow (Xe^{*+}, e^-) \rightarrow (Xe^{**}).$$

A photon driven excitation of the ion at the time when the freed electron is far away from the core could allow the formation of excited Xe^+ [e.g., $5s^2 5p^6(^2P)6s$, with 8 photons]. This process competes with an ionization of the ion [29]. After an excitation the rescattered electron can be recaptured and Xe^{**} will be subsequently ionized. (The energy of the rescattered electron is not enough to allow direct ionization.)

$$Xe^{**} + n \cdot \hbar\omega \rightarrow Xe^{*+} + e^-.$$

The freed electron can be used for further recollision processes allowing a stepwise transfer of laser energy to the atom. The dielectronic recombination increases the number of involved electronic states and could be the reason for the intensity yield dependence of electrons ejected at larger angles with respect to the polarization axis. CEIS measurements of Kr and Ar show similar features. The doubly charged ion is observed after the appearance of electrons from a NR ionization.

With the combined electron ion measurement we demonstrate the importance of the NR 9-photon ionization process for the formation of doubly charged xenon ions due to 800-nm, 100-fs short pulse laser interaction. According to a classical point of view the impact energy of rescattered electrons did not allow a direct ionization to doubly charged xenon and an excitation of Xe^+ from the ground state seems not to be possible. Dielectronic recombination could play a role in double ionization.

The authors thank A. Becker for the S-matrix calculation and H. Helm, C. J. G. J. Uiterwaal, and W. Kamke for stimulating discussions. The technical help of U. Person and I. Siegel is acknowledged. This work is supported by the SFB 276/C14 UPIII. B. W. is supported by DFG No. WI 1940/1-1.

*Electronic address: witzel@uni-freiburg.de

[1] A. L'Hullier *et al.*, Phys. Rev. A **27**, 2503 (1983).
[2] B. Walker *et al.*, Phys. Rev. Lett. **73**, 1227 (1994).
[3] D. N. Fittinghoff *et al.*, Phys. Rev. Lett. **69**, 2642 (1992).
[4] M. Lein *et al.*, Laser Phys. **12**, 487 (2002).
[5] L. Kamata *et al.*, Phys. Rev. Lett. **86**, 5687 (2001).
[6] M. Weckenbrock *et al.*, J. Phys. B **34**, L449 (2001).
[7] R. Moshammer *et al.*, Opt. Express **8**, 358 (2001).
[8] E. R. Peterson *et al.*, Phys. Rev. A **64**, 053405 (2001).
[9] D. Charalambidis *et al.*, Phys. Rev. A **50**, R2822 (1994).
[10] M.V. Ammosov *et al.*, Sov. Phys. JETP **64**, 1191 (1986).
[11] M. YU Kuchiev, JETP Lett. **45**, 404 (1987).
[12] M. YU Kuchiev, J. Phys. B **28**, 5092 (1995).
[13] P. B. Corkum, Phys. Rev. Lett. **71**, 1994 (1993).
[14] B. Witzel *et al.*, Phys. Rev. Lett. **85**, 2268 (2000).
[15] B. Witzel *et al.*, Eur. Phys. J. D **12**, 21 (2000)
[16] R. Lafon *et al.*, Phys. Rev. Lett. **86**, 2762 (2001).
[17] T. Weber *et al.*, Science **404**, 608 (2000).
[18] R. Kopold *et al.*, Phys. Rev. Lett. **85**, 3781 (2000).
[19] H. Helm *et al.*, Phys. Rev. Lett. **70**, 3221 (1993).
[20] C. Bordas *et al.*, Rev. Sci. Instrum. **67**, 2257 (1996).
[21] A. Talebpour *et al.*, J. Phys. B **30**, 1721 (1997).
[22] A. Becker *et al.*, Phys. Rev. A **59**, R3182 (1999).
[23] A. Becker *et al.*, J. Phys. B **32**, L335 (1999).
[24] G. G. Paulus *et al.*, J. Phys. B **29**, L249 (1996).
[25] H. Helm *et al.*, Phys. Rev. A **49**, 2767 (1994).
[26] V. Schyia *et al.*, Phys. Rev. A **57**, 3692 (1998).
[27] P. Hansch *et al.*, Phys. Rev. A **55**, R2535 (1997).
[28] A. Müller *et al.*, Phys. Rev. Lett. **56**, 127 (1986).
[29] K. C. Kulander *et al.*, Phys. Rev. A **51**, 561 (1995).